World Academy of Science, Engineering and Technology
International Journal of Mechanical and Materials Engineering
Vol:11, No:8, 2017

Laser Registration and Supervisory Control of neuroArm Robotic Surgical System

Hamidreza Hoshyarmanesh, Hosein Madieh, Sanju Lama, Yaser Maddahi, Garnette R. Sutherland, Kourosh Zareinia

***Abstract*—**This paper illustrates the concept of an algorithm to register specified markers on the neuroArm surgical manipulators, an image-guided MR-compatible tele-operated robot for microsurgery and stereotaxy. Two range-finding algorithms, namely time-of-flight and phase-shift, are evaluated for registration and supervisory control. The time-of-flight approach is implemented in a semi-field experiment to determine the precise position of a tiny retro-reflective moving object. The moving object simulates a surgical tool tip. The tool is a target that would be connected to the neuroArm end-effector during surgery inside the magnet bore of the MR imaging system. In order to apply flight approach, a 905-nm pulsed laser diode and an avalanche photodiode are utilized as the transmitter and receiver, respectively. For the experiment, a high frequency time to digital converter was designed using a field-programmable gate arrays. In the phase-shift approach, a continuous green laser beam with a wavelength of 530 nm was used as the transmitter. Results showed that a positioning error of 0.1 mm occurred when the scanner-target point distance was set in the range of 2.5 to 3 meters. The effectiveness of this non-contact approach exhibited that the method could be employed as an alternative for conventional mechanical registration arm. Furthermore, the approach is not limited by physical contact and extension of joint angles.

***Keywords*—**3D laser scanner, intraoperative MR imaging, neuroArm, real time registration, robot-assisted surgery, supervisory control.

I. Introduction

THE neuroArm neurosurgical robot is an image-guided Magnetic Resonance (MR)-compatible/safe system designed for both microsurgery and stereotaxy [1]. The system includes two robotic manipulators, a sensory-immersive workstation, a main system controller, and custom designed neurosurgical toolsets. Each neuroArm manipulator has six degrees of freedom (DOFs), remotely controlled by the surgeon located at a workstation adjacent to the operating room (OR). The manipulators are built from MR-compatible/safe materials including titanium, polyether ether ketone (PEEK), polyoxymethyline (Delrin®), together with titanium force sensors and ceramic actuators to minimize the effect on MR signal-to-noise (SNR). Prior to surgery, the robotic manipulators are registered for calibration and control of motion during the operation.

The current registration system for neuroArm consists of three main sub-systems: *registration arm*, *target assembly*, and *software*. The registration arm is a high-precision digitizing arm, which is used by the surgeon to touch specified points on the 3-pin headholder (patient) and the robotic manipulators [1]. Registration target assembly is referred to a device that is physically attached to the rigid skull fixation system (named also skull clamp) and has a fixed mechanical constraint on which fiducial markers are embedded. The registration software reads the Cartesian data points collected from the target assembly and touch points on the manipulator. The software then uses the data points to calculate centroids of the fiducials to determine the geometric relationship between the manipulator and the patient. When performing physical registration, the tip of the registration arm should gently touch the divots on both manipulators and targets [2]. Each touch point must be touched lightly as excessive pressure might move the unit or the head frame that could result in registration error. In addition, joints of the registration arm should not be locked in full extension when touching the fiducials. When positioning the neuroArm mobile base for microsurgery, the patient is placed in the skull clamp and upper arch with touch points, and registration markers are embedded in the upper skull clamp arc [3], [4]. Elements of a conventional registration system are shown in Fig. 1.

This study explores the development of a high-speed range-finding method for the neuroArm surgical system that facilitates the integration of precision and accuracy. Two important prerequisites of image-guided robotic surgery are *registration* and *supervisory control*. Registration allows the physical manipulator coordinate system to be linked to the MR image coordinate system [5]. Position control of the neuroArm manipulators during registration is currently carried out by a physical-contact registration system. This method is not only time-consuming but also is unable to guarantee the conservation of calibration accuracy during the operation. The excessive force that the operator might possibly apply when touching the markers adversely influences the registration accuracy. Upon completion of the registration, position of the tool-tip needs to be monitored accurately and continuously, when the manipulator is commanded to approach a specified area, e.g., a burr hole on the patient's skull. This supervisory control currently relies on the surgeon. For increased safety and accuracy, an improved and effective measurement of tool trajectory and motion would be beneficial. In this study, we hypothesized that the physical contact registration (before starting the operation) and supervisory control of a surgeon (during surgery) could be successfully replaced by a 3D laser scanner in the OR close to the magnet but outside the 5-Gauss

H. Hoshyarmanesh, S. Lama, Y. Maddahi, G. Sutherland, and K. Zareinia are with the Project neuroArm, Department of Clinical Neurosciences and Hotchkiss Brain Institute, University of Calgary, AB T2N 4Z6, Canada. (corresponding author, phone: 403-210-8175 fax: 403-210-9175, e-mail: hamidreza.hoshyarman@ucalgary.ca).

H. Madieh is with the Electrical Institute, Mohajer Technical and Vocational College, Isfahan, Iran.

line, reducing the need for MR compatibility. Amongst the existing methods for determining accurate position of a moving target, the laser range finder (LRF) was selected to speed up the registration procedure. The LRF also provides a high precision measurement [6].

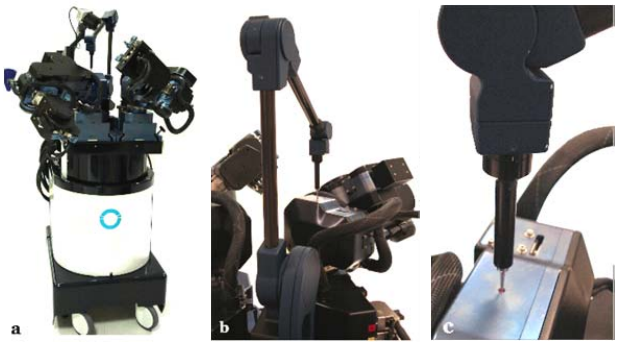

Fig. 1 (a) The neuroArm manipulator is being registered using a registration system, (b) Configuration of the digitizing arm, and (c) Digitizing probe with a ruby spherical tip touches a fiducial marker

Such a laser scanning system could well increase the safety of robot-assisted surgery by minimizing positioning errors, as it works in concurrence with other sensors. The system may also lead to a safer obstacle avoidance. Two range-finding algorithms: time-of-flight (ToF) and phase-shift (PS) are considered in this study. Implementation of a field-programmable gate array (FPGA) is also taken into account to apply a real-time control. The non-contact laser tracker diminishes the limitations of the conventional registration arm that require contact and are operator dependent.

II. Materials and Methods

Methods of implementing an LRF include Triangulation, Interferometry, Frequency Modulated Continuous Wave (FMCW), PS, and ToF [6]. The present work used PS and ToF. The PS method is a technique for measuring distances by sending a laser beam with sinusoidal modulated optical power to a target [7]. Some reflected beams, from diffuse or specular reflections, were monitored, and the phase of the power modulation was compared with that of the transmitted beam. One limitation of the technique is that the sine period for $\theta+2\pi n$ is not detectable, where $\theta=2\pi fn$ is a function of wave frequency (f) and time (t).

The ToF (or pulse measurements) is based on measuring the round trip time of flight of a laser pulse from the measurement device to/from a given target. This method is suitable for large distances [8], [9], and is the only method that is able to measure larger distances by increasing the power of the transmitter. In this study, an FPGA was used as the main processing unit for time-to-digital converter (TDC); however, to have an accurate and faster processor, full-custom design and standard-cell design are preferred to make an application-specific integrated circuit.

A. Time-of-Flight Approach (ToF)

The concept of measuring the flight time in the ToF technique is shown in Fig. 2. As observed, after the laser beam transmitted to a target, a start pulse activated TDC until the beam returned and triggered a stop pulse. During this process, the beam was flown for a distance of $2r$:

$$r = CN / (2 f_{clk}) \quad (1)$$

where, N is the number of counts, f_{clk} represents the clock frequency of the counter and C denotes the speed of light. The resolution of measurement or the minimum detectable difference in the distance, δ_r, is:

$$\delta_r = C / (2 f_{clk}) \quad (2)$$

1. Transmitter

A hybrid pulsed diode laser SPL LL90-3 with a wavelength of 905 nm and ability to produce pulse width less than 50 ns was chosen to increase safety during surgery. The output power was adjustable from 2 to 70 W corresponding to the charging voltage of 5 and 22 V, respectively. Using a proper driver for diode structure and ability to control frequency and pulse width, we were able to detect the target accurately [10]. The transmitter circuit is illustrated in Fig. 3.

2. Receiver

Using a lens to concentrate and filter the retuning beam is important, as the reflected beam is not concentrated after reflection. Tolerance to temperature fluctuations should be close to zero. In the current study, thermoelectric control module controls an Avalanche Photo Diode (APD) temperature to receive appropriate response with minimum tolerance. The APD driver needs a high voltage power supply to make the reverse voltage of 400 V and have the photo diode working in avalanche area. The receiver works with a maximum wavelength of 905 nm. Since TDC requires Transistor-Transistor-Logic (TTL) signal to operate, the received signals by the receiver must be converted to TTL level with appropriate width by a comparator circuit as shown in Fig. 4.

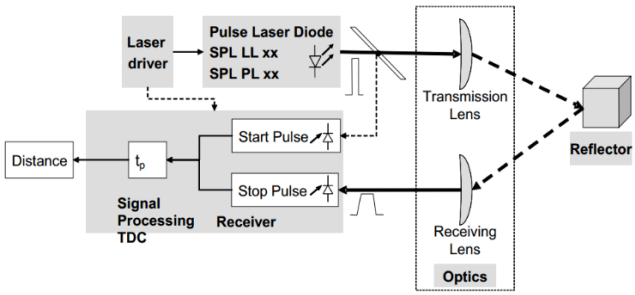

Fig. 2 ToF, transmitter and receiver concept in an LRF [8], [9]

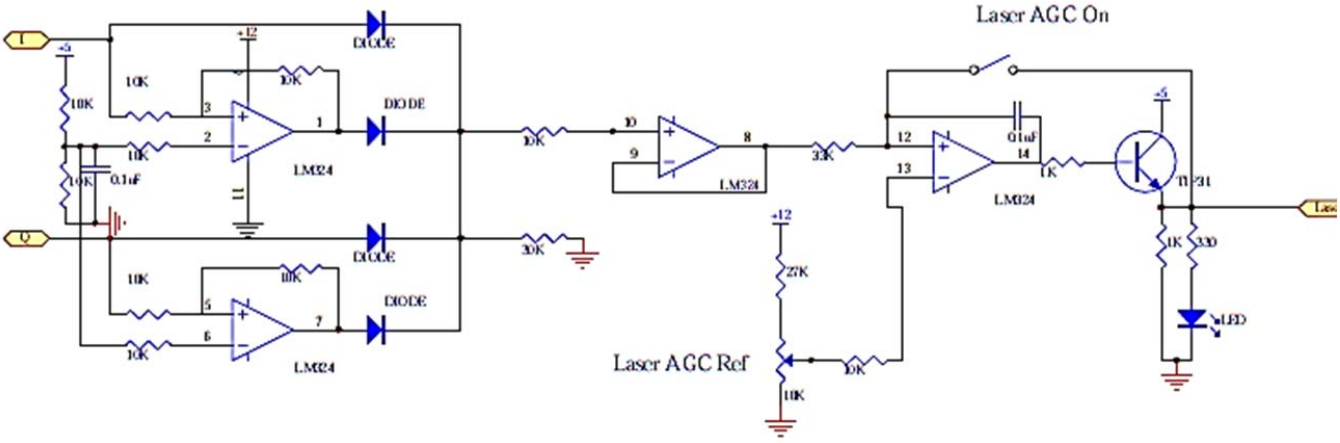

Fig. 3 Transmitter circuit composed of signal generator, laser driver and laser photo diode

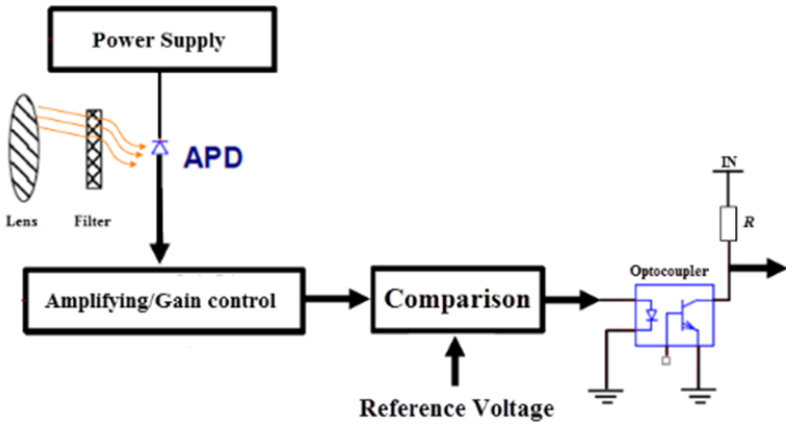

Fig. 4 Comparator circuit modeled to modify the received signal

Power of reflected signal (P_{in}) is directly proportional to the transmitter power (P_{out}), and has an inverse relationship with the distance squared (r^2) as follows [8], [9]:

$$P_{in} = (\rho \tau S / (\pi r^2)) P_{out}$$
$$\tau = \tau_c \tau_{out} \quad (3)$$

where S is the area of optical receiver, $\boldsymbol{\tau}$ denotes the transmission coefficient of environment, which is equal to product of transmission coefficient of the optics ($\boldsymbol{\tau_{out}}$) and the medium ($\boldsymbol{\tau_c}$). ρ represents the beam scattering in terms of the color of the target (i.e., for a perfect reflecting surface is equal to 1 and for a zero-reflecting surface is considered as zero) [8]–[11]. The output voltage of laser receiver was calculated using (4).

$$V_0 = P_{in} R Z_t A_v \quad (4)$$

In (4), P_{in} is the received signal power from reflected beam, Z_t denotes the transmission impedance, R is the sensitivity coefficient, and A_v is the gain factor.

3. Time-to-Digital Converter (TDC)

TDC is a high frequency counter that calculates the time-of-flight from transmitter to receiver (incident and reflected beam) [12]. By using Clock Wizard, a tool in ISE software, different frequencies are generated in output from a reference frequency [12]–[14]. Although TDC is structured as a high frequency counter, the maximum error in calculations could be considered equal to one clock width shown in Fig. 5. In (5), $error_1$ affects the start pulse and makes error by only increasing the true value, whilst $error_2$ is generated in stop pulse and causes error by solely decreasing the true value. This was the principle behind considering $error_2$ with negative sign.

$$T_m = error_1 + T_{12} - error_2 = nT_{clk} + T_1 - T_2 \quad (5)$$

4. Measuring the Exact Distance

a) Ring Oscillator

The main difference of TDC architectures is their interpolations. Since only digital circuits are implemented on FPGAs, digital parameters must be applied for interpolations. Among various digital interpolation techniques, the Vernier [14] was used in this research as follows.

$$Error_{T1} = (n_1 - 1)T_{slow} - (n_2 - 1)T_{fast} \quad (6)$$

where n_1 is the number of counts for slow oscillator, and n_2 is

for the fast. Main structure of this method is based on two high frequency oscillators. As depicted in Fig. 6, the frequency ranges are very close. At rising edges of $error_1$, the slow oscillator is activated and a counter starts counting its clock pulses. When falling edges of $error_1$ happens, fast oscillator is activated and oscillation of both oscillators will continue to the point of being in phase [12], [13]. Oscillating frequency depends on internal design and hardware delay.

$$T_{Resolution} = T_{slow} - T_{fast} \quad (7)$$

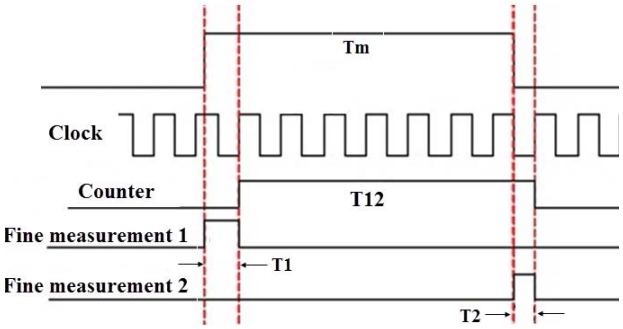

Fig. 5 Architecture of time measurement in TDC

b) Double Oscillator

There are various methods for creating multi-rate oscillations [15]–[18]. Fig. 7 depicts a double oscillator with two different oscillation rates.

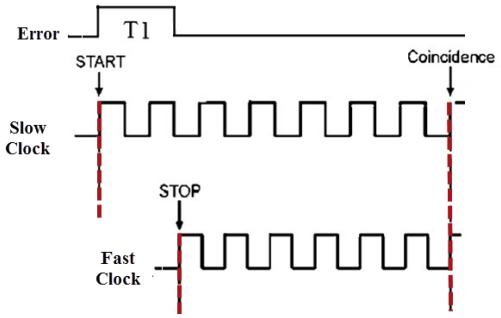

Fig. 6 Fast and slow oscillators simulated to evaluate the ring oscillator

5. Phase Detector (PD)

After starting both oscillators, a circuit should be designed to ascertain that the oscillators are in phase. In fact, this circuit detects in phase situation by focusing on both edges of signal and using digital edge detection technique.

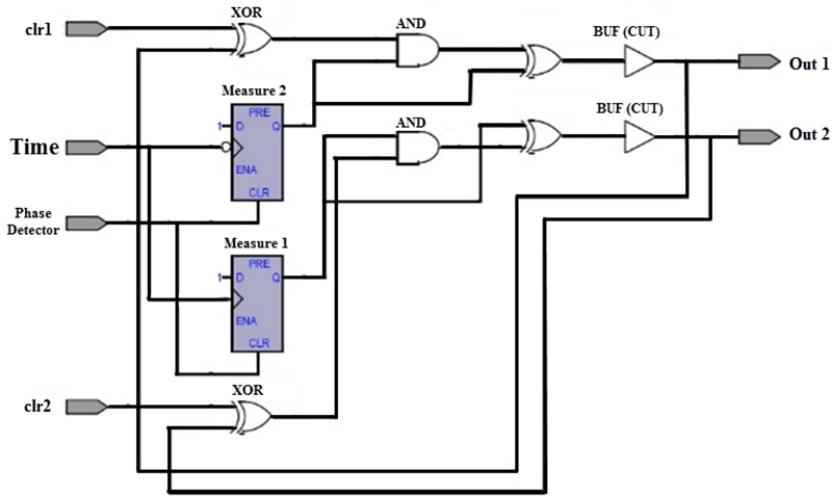

Fig. 7 A controllable double oscillator used to change the oscillation rate

6. Noise Analysis

As mentioned above, ToF is a high frequency method. Moreover, reflected laser signal has low power in range of nW. Thus, it is prone to noise at high frequencies. The following equations indicate how SNR defines the system accuracy [19], [20]. For a repetition rate of N=1, we have:

$$\delta_d = 0.35C / (2\Delta_{fi} SNR) \quad (8)$$

$$\Delta_{fi} = BW \approx 0.35 / t_r \quad (9)$$

and, for a repetition rate of 1< N <15, it changes into:

$$\delta_d = 0.35C / (2\sqrt{N}\Delta_{fi} SNR) \quad (10)$$

In (8)-(10), Δ_{fi} is the frequency bandwidth, and C denotes the speed of light. There are some methods to decrease noise in a LRF by appropriate design. For example, noise created by laser switching drive can be reduced by an electromagnetic interface filter. Separating earth link from the analog receiver can also filter digital noises. Although the system noise is generally related to receiver circuit, other parts also have noisy signals that could be reduced by using an opto-coupler. At the time of receiving reflected laser signal, all sources of noise must have minimal effect.

B. Phase-Shift Method

The fundamental principle of laser phase-shift range-finder is based on the modulation of sine-wave amplitude. If f_0 is the modulation frequency, and $\Delta\varphi$ the measured phase-shift between the reference signal emitted by a continuous laser diode and the optical signal reflected from the target, then d can be calculated using [21]:

$$\Delta\varphi = 4\pi f_0 d / C \tag{11}$$

Although the PS method was studied and simulated so as to evaluate its accuracy for implementation in the surgical application, ToF was employed for the experiments.

III. Experimental Details

The 3D laser scanner, used for registration, is able to digitize the position of the manipulator and surgical tool-tip in a quick and non-contact manner. The process takes a few seconds. High acceleration movement of such a mechanism is provided by a prismatic joint along Z_0 and two low friction rotational joints around X_0 and Z_0, as depicted in Fig. 8. The scanner lens –with diameter of 45 mm and canonical distance of 70 mm– is equipped with a green filter. The actuators are two accurate stepper motors with the resolution of 0.36 degree per pulse controlled in micro-stepping mode. At the beginning, laser beam detects the target points designated by retro-reflective sheets, while the laser head is scanning the initial configuration of the target within its cylindrical workspace. The robotic manipulator is kept stationary during initial registration, and the microsurgery tool attached to the end effector is assumed to have a very low speed during stereotaxy inside the magnet bore. The laser scanner base is fixed in the OR close to both manipulator and magnet in a safe magnetic zone (<5 Gauss) with maximal reachability, i.e. no obstacles in the line-of-sight.

The laser scanner is currently being considered as an adjunct to robot-assisted microsurgery and stereotaxy. In image-guided surgery, the surgeon uploads patient 3D MR images on to a workstation. The surgical manipulators are registered to the 3D images that include tool overlay. While using precise digital encoders and kinematic chain formulations of the manipulator provides an accurate and precise location of the end-effector of the robot, some errors might occur due to unforeseen circumstances, e.g. brain shift, encoder or connector failure. Supervising and following the displacement of the end-effector by a non-contact laser tracker, can provide an additional layer of safety to the robot-assisted procedures when the robot is working in semiautonomous mode. The problem of brain shift is overcome by repeating MR imaging with re-registration.

The laser scanner records the coordinate of the target points to be consolidated with the obtained imaging data. Laser application could also be applied to robotic tele-surgical systems with a haptic interface in which real-time images are received from the surgical site while the surgeon controls the robot. Since the robotic manipulators replicate the surgeon's motions at the human machine interface in a master-slave paradigm, errors due to hardware or software failure, patient or equipment motion, or operator mistake, could result in inadvertent motion. The measured errors by laser scanner incorporated with encoder readings and other sensors in a closed loop control, provide a novel risk mitigation strategy independent of the robotic system.

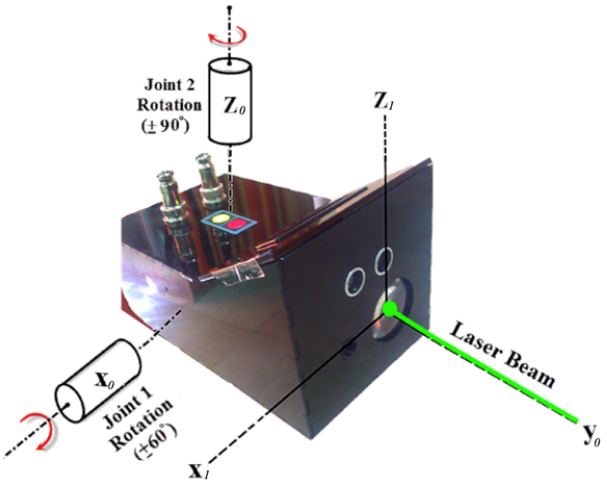

Fig. 8 The 3D Laser scanner designed and developed for registration and supervisory control of neuroArm manipulator

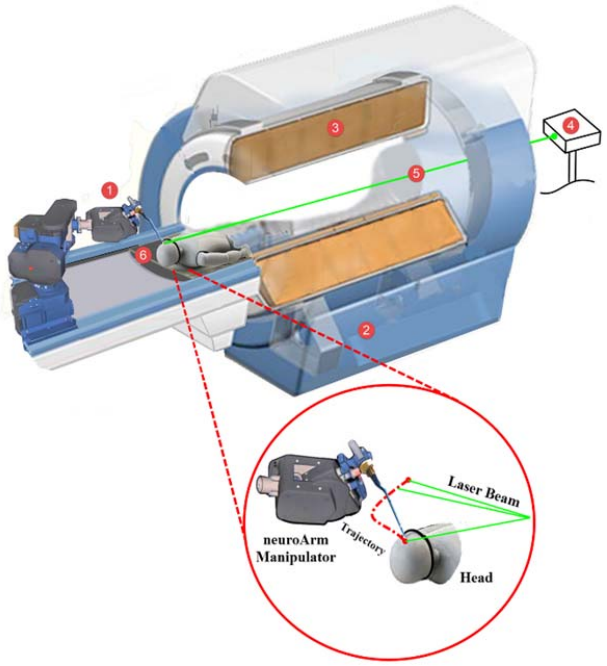

Fig. 9 Laser scanner application in an iMRI surgery, 1) neuroArm manipulator, 2) MRI scanner, 3) Magnet, 4) Laser scanner, 5) Laser beam, and 6) Patient's head

This supervisory control ensures that the robotic manipulator moves along the path preplanned by the surgeon. Fig. 9 illustrates how the manipulator could be tracked and controlled when an intraoperative stereotaxy is being performed. In this figure, neuroArm manipulator and patient

are illustrated *just outside* the magnet bore for better visualization of configuration details; however, the proposed operation takes place inside the magnet bore [22], [23]. A laser head with a high resolution of 32 microsteps at 0.36 DPP could be applied to track the tool within the Cartesian coordinate system.

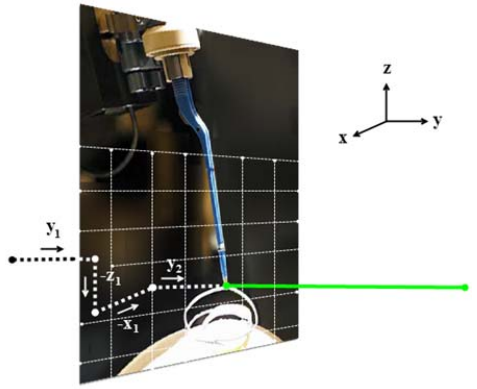

Fig. 10 Tool path tracking of forceps tip by laser beam in Cartesian coordinate system

Several tests are considered according to Fig. 10 to alleviate the challenges of supervisory control of a pair of bipolar forceps. Prior to conducting tests in the OR, an initial experiment was set up to simulate the registration process, followed by a second experiment that simulated the physical movement of a surgical tool. A small retroreflective target was selected, initially stationary and then moving, as a flying object with a slow speed in X-Y plane for the first and second experiments, respectively. The laser scanner measured and recorded the exact position of the fixed and moving targets within the 3D space. The tool path was projected along X, Y, and Z axes.

IV. Results

To project a laser beam from the transmitter to the target, a frequency sample was generated at 300 kHz from a 100-kHz reference signal [13]. The signal, simulated in iSim software, showed how the central counter worked and generated errors (see Fig. 11). In the ToF approach, two methods were utilized to minimize the errors and the figure illustrates the positive effect of both. First, the processing unit frequency was increased to have higher counting frequency and less error, i.e. doubling the frequency cuts the error in half. In practice however, the maximum frequency of the system would be limited by the hardware design and the microprocessor. An alternative approach would be to use an error detection technique, where the frequency selected of 300 kHz in Vernier approach [14], would decrease the error by 1/20, with equal or less expense compared to the first method. The resolution for the applied ring oscillator was also simulated and compared with (7) as depicted in Fig. 12.

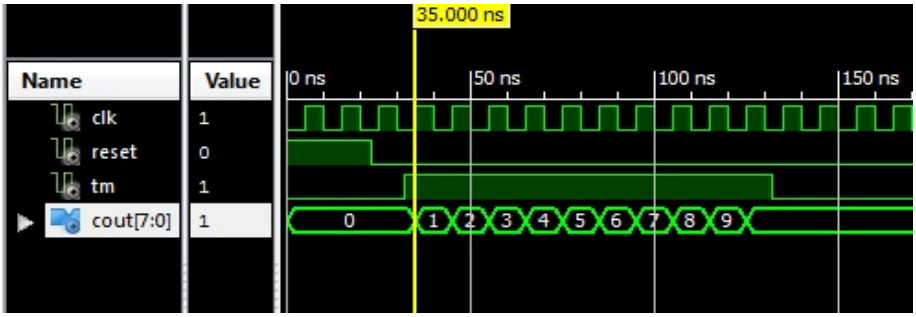

Fig. 11 Simulation result of transmission signal in iSim

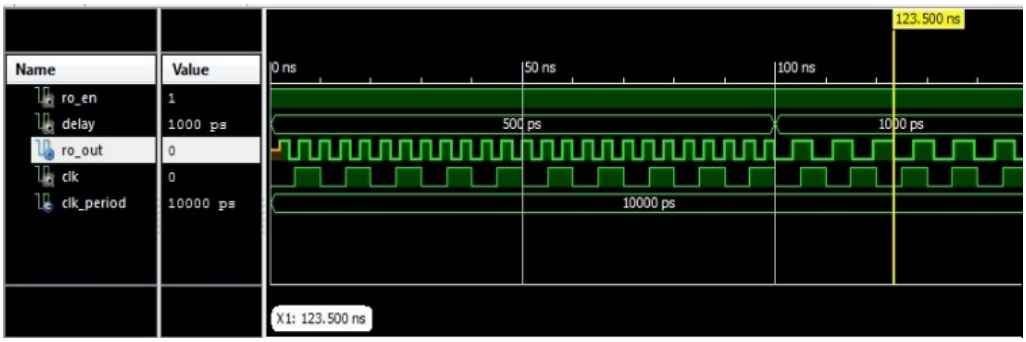

Fig. 12 Simulation result of ring oscillator with different gap delays

Additional experiments were performed to measure the accuracy of the system and investigate applicability of the system to the OR scenario. Figs. 13 (a) and (b) show the scanning procedure before and after determination of the exact position of a moving object in X-Y plane. Laser beam normally finds the object after sweeping X-Y plane for each Z

level in multiple iterations. Tracking along X and Z constitutes higher error values in comparison to Y axis, as they are lateral directions perpendicular to the laser beam. The mean errors along X and Z are in the order of 1 mm at the distance of r=2m between the sample target and the emitter lens of the scanner. The error would be less than 0.4 mm along Y at the same conditions. The results, listed in Table I, show a few positioning errors (δ_d) for a moving target similar to forceps in a surrounded environment at different longitudinal distances (along y direction) and rotational angles around Z axis (θ).

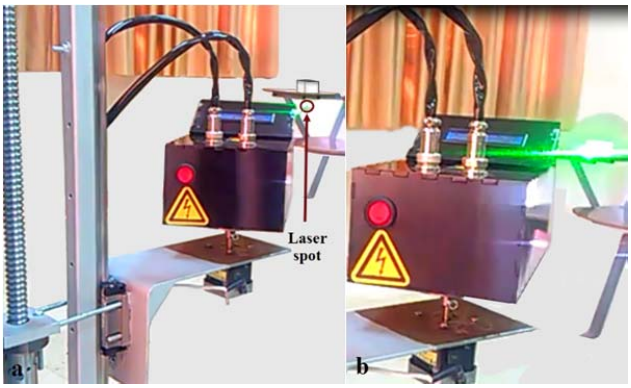

Fig. 13 Tracking procedure, (a) before finding, and (b) after finding and stopping at the cylindrical coordinate of the moving target

TABLE I
POSITIONING ERROR FOR THE MOVING TARGET AT DIFFERENT LONGITUDINAL DISTANCES AND ANGLES

Test no.	r (mm)	θ (degree)	Error δ_d (mm)
1	632.20	30,60	0.17
2	1414.04	42	0.47
3	2788.02	56	0.10
4	3873.03	102	0.18

V. CONCLUSION

3D laser scanner is a novel optoelectronic device, which has the potential to be used for robot-assisted microsurgery and stereotaxy allowing registration and supervisory control of the manipulators. The non-contact method is an advantage over conventional registration techniques that are contact-based [24]. The results further show that the laser scanner system can potentially minimize the effect of inadvertent motion by providing a trajectory tracking mechanism independent of the robotic system. This study is believed to make further contribution to the registration and supervisory control of semiautonomous robotic manipulators, especially in medical applications, where a high level of safety is mandatory and patient injury must be avoided. The method of registration in this study is practical and can lead to improvement in wide variety of applications of medical/surgical robotics, potentially replacing conventional mechanical registration arm. Furthermore, the technique, with more sensitive receivers and low intensity lasers, offers the ability to quantify brain shift and thereby offering a seamless and real time ability to re-register existing navigation systems during surgery.

REFERENCES

[1] Y. Maddahi, K. Zareinia, L. S. Gan, S. Lama, G. R. Sutherland, and N. Sepehri, "Positional and force characteristics of neuroArm robotic manipulators: A pilot study," *Int. Conf. of Control, Dynamic Systems, and Robotics*, Ottawa, Canada, 2015.

[2] G. R. Sutherland, I. Latour, and A. D. Greer, "Integrating an image guided robot with intraoperative MRI: A review of design and construction," *IEEE Eng. Med. Biol.*, vol. 27, pp. 59–65, 2008.

[3] Y. Maddahi, L. S. Gan, K. Zareinia, S. Lama, N. Sepehri, and G. R. Sutherland, "Quantifying workspace and forces of surgical tools during robot-assisted neurosurgery," *Int. J. Med. Robotics Comput. Assist. Surg.*, vol. 12, no. 3, pp. 528–37, 2016.

[4] A. D. Greer, P. Newhook, and G. R. Sutherland, "Human-machine interface for Robotic Surgery and Stereotaxy," *IEEE/ASME Trans. on MRI Compatible Mechatronic Systems*, vol. 13, pp. 355–361, 2008.

[5] Y. Maddahi, K. Zareinia K, L. S. Gan, S. Lama, G. R. Sutherland, N. Sepehri, "Positional and force characteristics of neuroArm robotic manipulators: a pilot study.," in *Proc. Intern. Conf. of Control, Dynamic Systems and Robotics*, Ottawa, 2015.

[6] M. C. Amann, T. Bosch, M. Lescure, R. Myllyla, M. Rioux, "Laser ranging: a critical review of usual techniques for distance measurement", *Opt. Eng.*, vol. 40, no. 1, pp. 10–19, 2001.

[7] Y. Bae, "An Improved Measurement Method for the Strength of Radiation of Reflective Beam in an Industrial Optical Sensor Based on Laser Displacement Meter", *Sensors*, vol. 16, no. 5, pp. 752, 2016.

[8] S. Mohammad Nejad and S. Olyaee, "Comparison of TOF, FMCW and phase-shift laser range finding methods by simulation and measurement," *J. Tech. Educ.*, vol. 1, no. 1, pp. 11–18, 2006.

[9] S. Mohammad Nejad and S. Olyaee, "Low-noise high-accuracy TOF laser range finder," *Am. J. Appl. Sci.*, vol. 5-7, pp. 755–762, 2008.

[10] S. Mohammad Nejad and S. Olyaee, "Unified pulsed laser range finder and velocimeter using ultra-fast time-to-digital converter," *Iranian J. Elect. Electron. Eng.*, vol. 5, no. 2, pp. 112–121, 2009.

[11] Photon Detection Datasheet, C30659 Series-Rev.1.1, pp. 1–10, 2013. www.excelitas.com.

[12] J. Song, Q. An, and S. Liu, "A high-resolution time-to-digital converter implemented in field-programmable-gate-arrays," *IEEE Trans. Nuclear Science*, vol. 53, no. 1, pp. 236–241, 2006.

[13] M. C. Lin, G. R. Tsai, C. Y. Liu, and S. S. Chu, "FPGA-based high area efficient time-to-digital IP design," in *TENCON IEEE Region 10 Conf.*, Hong Kong, 2006, pp. 1–4.

[14] M. P. Mattada, and H. Guhilot, "Area efficient vernier time to digital converter (TDC) with improved resolution using identical ring oscillators on FPGA," in *IEEE Int. Conf. Smart Struct. Syst. (ICSSS),* Chennai, 2013, pp. 125–130.

[15] J. Wang, S. Liu, Q. Shen, H. Li, and Q. An, "A fully fledged TDC implemented in fieldprogrammable-gate-arrays," *IEEE Trans. Nuclear Science*, vol. 57, no. 2, pp. 446–450, April 2010.

[16] J. Kostamovaara, S. Kurtti, and J. P. Jansson, "A receiver – TDC chip set for accurate pulsed Time-of-flight laser ranging," *CDNLive EMEA Conf. Proc.*, Munich, 2012.

[17] F. Zhong, L. Wan, and Y. Yue, "High-precision interval measuring chip TDC-GP2 in accurate distance measuring," *Comp. Indust. Control*, vol. 4, pp. 69–72, 2007.

[18] A. Aloisio, P. Branchini, R. Cicalese, R. Giordano, V. Izzo, and S. Loffredo, "FPGA implementation of a high-resolution time-to-digital converter," in *IEEE Nuclear Science Symposium Conference Record*, 2007, pp. 504–507.

[19] J. Kalisz, R. Szplet, J. Pasierbinski, and A. Poniecki, "Field programmable gate array based time-to-digital converter with 200-ps resolution", *IEEE Trans. Instrum. Meas.*, vol. 46, no.1, pp 51–55, Feb. 1997.

[20] P. Dudek, S. Szezepanski, and J. Hatfield, "A high resolution CMOS time-to-digital converter utilizing a Vernier delay loop," *IEEE Trans. Solid State Circuits*, vol. 35, no. 2, pp. 240–247, 2000.

[21] S. Poujouly, B. Journet and D. Placko, "Digital laser range finder: phase-shift estimation by undersampling technique," *Indust. Electron. Society, The 25th Annu. Conf. IEEE*, San Jose, CA, vol. 3, 1999, pp. 1312–1317.

[22] T. Y. Cossetto, K. Zareinia and G. R. Sutherland, "Neurosurgery," in *Surgical Robotics*, vol. 3, P. Gomes, Ed. Cambridge: Wood Head Publishing Ltd., pp. 59-77, 2012.

[23] G. R. Sutherland, S. Wolfsberger, S. Lama, K. Zareinia. "The Evolution of neuroArm," *Neurosurgery*, vol. 72, pp. A27–A32, 2013.

[24] A. Mert, L. S. Gan, E. Knosp, G. R. Sutherland, S. Wolfsberger, "Advanced Cranial Navigation," *Neurosurgery*, vol. 72, pp. A43-A53, 2013.